Spin Seebeck effect in the classical easy-axis antiferromagnetic chain

X. Zotos

Department of Physics, University of Crete, 70013 Heraklion, Greece
and Max-Planck-Institut für Physik Komplexer Systeme, 01187 Dresden, Germany

By molecular dynamics simulations, we study the spin Seebeck effect as a function of magnetic field in the prototype classical easy-axis antiferromagnetic chain, far out of equilibrium as well as linear response regime. We find distinct behavior in the low-field antiferromagnetic, middle-field canted, and high-field ferromagnetic phase. In particular, in the open boundary system at low temperatures, we observe a divergence of the spin current in the spin-flop transition between the antiferromagnetic and canted phase, accompanied by a change of sign in the generated spin current by the temperature gradient. These results are corroborated by a simple spin-wave phenomenological analysis and simulations in the linear response regime. They shed light on the spin current sign change observed in experiments in bulk antiferromagnetic materials.

I. INTRODUCTION

The generation and control of spin currents is a central topic in the field of spintronics [1]. In particular, the spin Seebeck effect [2], the generation of a spin current by a temperature gradient in a magnetic field, has been extensively studied experimentally and theoretically in a great variety of bulk magnetic systems, for instance, the ferrimagnetic YIG/Pt heterostructures, antiferromagnetic materials (e.g., Cr_2O_3, Fe_2O_3), and van der Waals two-dimensional (2D) materials such as the quasi-2D layered ferromagnets, $Cr_2Si_2Te_6$ and $Cr_2Ge_2Te_6$ (for an extensive review, see Ref. [1]). In particular, concerning easy-axis bulk antiferromagnetic materials, there is experimental [3–6] and theoretical [7–10] interest and debate concerning the sign of the generated spin current [2,11].

In a different research domain, the physics of (quasi-)one-dimensional magnetic systems, both classical and quantum, has been studied for years, starting with the Bethe ansatz solution of the antiferromagnetic spin-1/2 chain. In particular, the exotic physics of easy-axis antiferromagnetic spin chains [12] and quantum spin-liquid materials with topological spinon excitations has attracted great interest. The spin Seebeck effect in the spin-1/2 chains Sr_2CuO_3 with spinon and $CuGeO_3$ with triplon excitations has been studied experimentally [13,14] and rigorously evaluated theoretically [15] in the easy-plane regime. Furthermore, the thermal transport of classical spin chains has been studied by numerical dynamics simulations [16], and lately the character of spin transport, i.e., ballistic, diffusive, or anomalous, in classical and

quantum (anti-)ferromagnetic chains has attracted a great deal of attention (for a recent tour de force and references therein, see [17]).

Here we study the spin Seebeck effect for the easy-axis classical antiferromagnetic spin chain; it makes sense to try to understand the physics of the effect in this prototype, but realistic model. It allows us to clarify the relation of the sign of the induced spin current by a temperature gradient across the spin-flop transition occurring at a critical field and serves as a bridge between spintronics studies in bulk materials and model magnetic systems. Besides the academic interest, quasi-one-dimensional compounds exist that can offer a platform for obtaining spin currents besides the bulk materials that are usually studied.

In the following, we first employ standard molecular dynamics (MD) simulations [18] to study the out-of-equilibrium spin current generation by a thermal current in a magnetic field. We find a sign reversal of the spin current at the critical field between the antiferromagnetic and canted ferromagnetic phase that we analyze by a simple spin-wave theory. The divergence of the induced current at the spin-flop transition could be observed in large spin quasi-one-dimensional spin chain compounds. The picture of the far-out-of-equilibrium spin Seebeck effect is corroborated by a simple spin-wave phenomenological model and simulations in the linear response regime.

II. MODEL

The model we study is the classical antiferromagnetic Heisenberg chain with easy-axis anisotropy given by the Hamiltonian

$$H = \sum_{l=1}^{L} J_\perp \left(S_l^x S_{l+1}^x + S_l^y S_{l+1}^y \right) + \Delta S_l^z S_{l+1}^z - h S_l^z, \quad (1)$$

---

where $\mathbf{S_l}$ is a unit vector with components $S_l^{x,y,z}$, $J_\perp > 0$ is the in-plane and $\Delta > 0$ the easy-axis exchange interactions with $\Delta > J_\perp$ and h the magnetic field. We will use the common parametrization $S_l^x = \sin\theta_l\cos\phi_l$, $S_l^y = \sin\theta_l\sin\phi_l$, $S_l^z = \cos\theta_l$.

The spin dynamics is given by Landau-Lifshitz equations of motion,

$$\frac{d}{dt}\mathbf{S_l} = \mathbf{S_l} \times \left(-\frac{\partial H}{\partial \mathbf{S_l}}\right). \tag{2}$$

To study far-out-of-equilibrium transport, we use a straightforward numerical method, simulating the microscopic heat transfer by embedding the spin system between two Langevin thermostats at temperatures T_L, T_R, realized by two Heisenberg chains of length N_L, N_R. We apply the Heun method [18] to numerically integrate the stochastic version of the Landau-Lifshitz-Gilbert equation for magnetic systems,

$$(1+\alpha^2)\frac{d}{dt}\mathbf{S_l} = \mathbf{S_l} \times \left(\xi_l - \frac{\partial H}{\partial \mathbf{S_l}}\right) - \alpha\mathbf{S_l}\left[\mathbf{S_l} \times \left(\xi_l - \frac{\partial H}{\partial \mathbf{S_l}}\right)\right], \tag{3}$$

where α is a damping coefficient and ξ_l a white Gaussian noise representing the thermostat at temperature T,

$$\langle\xi_l(t)\rangle = 0, \quad \langle\xi_l(t_1)\xi_k(t_2)\rangle = 2\alpha T\delta_{lk}\delta(t_1-t_2).$$

The spin J^S and energy J^E currents are given by the corresponding spin and energy continuity equations [19,20],

$$J^S = \sum_l J_\perp\left(S_l^x S_{l+1}^y - S_l^y S_{l+1}^x\right), \tag{4}$$

$$J^E = -\sum_l J_\perp^2\left(S_{l-1}^x S_l^z S_{l+1}^y - S_{l-1}^y S_l^z S_{l+1}^x\right)$$
$$- J_\perp\Delta S_{l-1}^z\left(S_l^x S_{l+1}^y - S_l^y S_{l+1}^x\right)$$
$$- J_\perp\Delta\left(S_{l-1}^x S_l^y - S_{l-1}^y S_l^x\right)S_{l+1}^z. \tag{5}$$

We first establish the phase diagram, in the zero-temperature limit, by considering the high-field region where $\theta_l = \theta$, $\phi_{l+1} - \phi_l = \pi$, obtaining, by minimization of the energy,

$$E_{\text{ferro}} = -J_\perp\sin^2\theta + \Delta\cos^2\theta - h\cos\theta,$$

$$z \equiv \cos\theta = \frac{h}{2(J_\perp+\Delta)}. \tag{6}$$

The critical field $h_f = 2(J_\perp + \Delta)$ above which we have the ferromagnetic phase is obtained setting $z = 1$. The critical magnetic field h_c, above which we have a canted ferromagnetic phase and below an antiferromagnetic one with $\theta_{l+1} - \theta_l = \pi$, is obtained by equating the energies of the two states,

$$E_{\text{ferro}} = E_{\text{afo}} = -\Delta, \quad h_c = 2\sqrt{\Delta^2 - J_\perp^2}.$$

III. MD RESULTS

In Fig. 1, we show the ratio of the mean spin current $\langle J^S\rangle$ to the mean thermal current $\langle J^Q\rangle = \langle J^E\rangle - h\langle J^S\rangle$. The mean values, $\langle O\rangle = \frac{1}{L}\langle\sum_l O_l\rangle$, O_l a local quantity, are obtained by averaging over about 10^8 samples by sweeping over all lattice sites (we take $N_L = N_R = L/2$). The thermal current
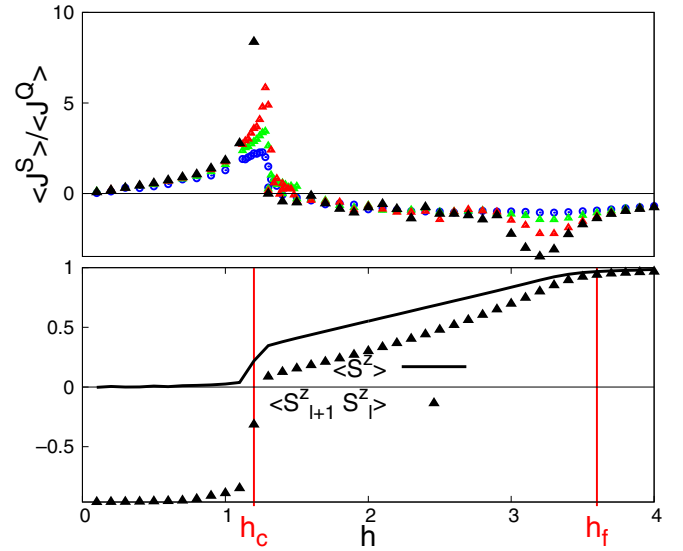

FIG. 1. Ratio of spin to thermal current as a function of magnetic field for $J_\perp = 0.8$. The mean $(T_L + T_R)/2$ temperature is $T = 0.02$ and the system sizes $L = 160$ (blue), 320 (green), 640 (red), 1280 (black). Also shown below are the mean magnetization (black line) and nearest-neighbor spin-spin correlation (black triangles).

is induced by setting the left (right) baths at different temperatures T_L (T_R), creating a constant temperature gradient along the chain. In the middle of the chain ($l = 1, L$), the damping coefficient α and the white Gaussian noise ξ_l are set equal to zero. The mean temperature is $T = 0.02$, with up to $T_L = 0.03$, $T_R = 0.01$. Here, $J_\perp = 0.8$ and we take $\Delta = 1$ as the unit of energies and temperature, implying critical fields $h_c = 1.2$, $h_f = 3.6$.

Concerning the numerical simulation, we find that the results are essentially independent of the temperature gradient within the accuracy of the simulation. The thermal gradient induces a thermal current, which in turn induces a spin current. Being a second-order effect, the measured spin current shows rather large fluctuations in the data compared to the thermal current. Thus we use relatively large temperature gradients to improve the accuracy of the data. In the particular simulations, we used, as baths, isotropic antiferromagnetic Heisenberg chains ($J_\perp = \Delta = 1$) in a zero magnetic field for which the energy-temperature relation is known. However, we found that the use of other baths, e.g., a ferromagnetic chain or a phonon bath, does not qualitatively change the spin current–thermal current relation.

The most notable feature in the data in Fig. 1 is the sharp reversal of the spin current at the spin-flop transition (to be discussed later in the framework of a spin-wave theory) and the size dependence indicating a diverging spin current in the zero-temperature limit. In the low-field antiferromagnetic phase, the spin current is in the same direction as the thermal current, while in the ferromagnetic one, it is opposite to the thermal current. Of course, as expected, reversing the direction of the magnetic field reverses this relation. In the second part of the figure (below), we show the magnetic field dependence of the average magnetization $\langle S^z\rangle$ and nearest-neighbor
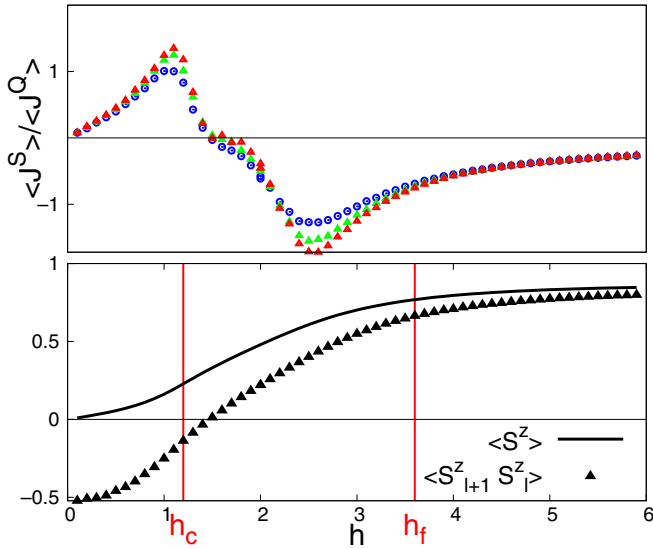
FIG. 2. Ratio of spin to thermal current as a function of magnetic field for $J_\perp = 0.8$. The mean $(T_L + T_R)/2$ temperature is $T = 0.2$ and the system sizes $L = 160$ (blue), 320 (green), 640 (red). Also shown below are the mean magnetization (black line) and nearest-neighbor spin-spin correlation (black triangles).

spin correlation $\langle S_{l+1}^z S_l^z \rangle$, clearly indicating the development of the three magnetic phases.

In Fig. 2, we show the same quantities at a higher temperature, where the transitions are smoothed out but the same features remain. Also, the finite-size effects are reduced as well as the ratio of the spin to thermal current, in relation to the temperature increase.

In Fig. 3, we show the field dependence of the spin and thermal conductivities separately. While the thermal current shows anomalies at the spin-flop and ferromagnetic transition,
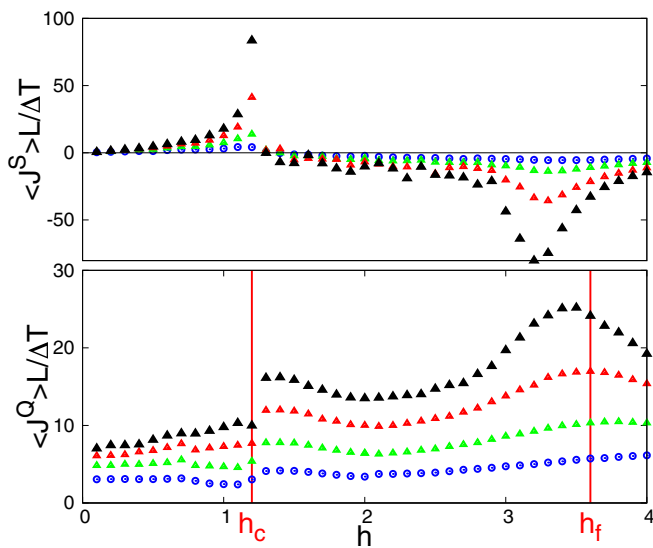

FIG. 3. Spin and thermal conductivities as a function of magnetic field for $J_\perp = 0.8$. The mean $(T_L + T_R)/2$ temperature is $T = 0.02$ and the system sizes $L = 160$ (blue), 320 (green), 640 (red), 1280 (black).
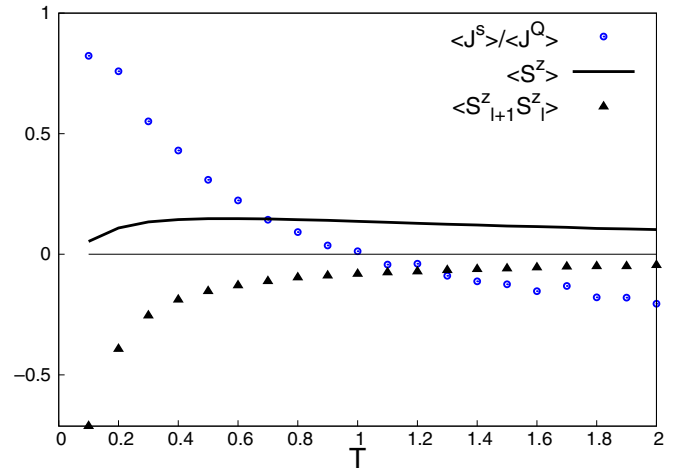

FIG. 4. Ratio of spin to thermal current, magnetization, and nearest-neighbor correlations as a function of temperature for a magnetic field $h = 0.8$ and $L = 160$.

the spin current is clearly responsible for the sign changes and overall behavior shown in Fig. 1.

Finally, in Fig. 4, we show the temperature dependence of the spin Seebeck effect by the ratio $\langle J^S \rangle / \langle J^Q \rangle$ at $h = 0.8$. In this field, we are at the antiferromagnetic regime at low temperatures and the sign of the ratio is positive. Raising the temperature, the antiferromagnetic phase "melts" with the appearance of an increasing number of domain walls, until a critical temperature $T \sim 1$ where we observe a change to a negative sign of the spin current, as in the ferromagnetic regime. To get an insight into this picture, we show the temperature dependence of the uniform magnetization, which is rather small at this field, and the decreasing nearest-neighbor antiferromagnetic spin-spin correlations.

IV. SPIN-WAVE ANALYSIS

We can reach an understanding of the spin current sign reversal and divergence at the spin-flop transition by considering a simple linear spin-wave theory. First, in the high-field $|h| > h_c$ canted ferromagnetic phase, linearizing in S_l^x, S_l^y the equations of motion (2), we obtain

$$\dot{S}_l^x = -S_l^y(2\Delta z - h) + z J_\perp \left(S_{l+1}^y + S_{l-1}^y \right),$$
$$\dot{S}_l^y = +S_l^x(2\Delta z - h) - z J_\perp \left(S_{l+1}^x + S_{l-1}^x \right)]$$

(the dot indicating the time derivative). With the substitution

$$S_l^x \pm i S_l^y = u e^{i(ql - \omega_\pm t)}, \tag{7}$$

we obtain the spin-wave spectrum,

$$\omega_\pm = \pm h \mp 2z(\Delta - J_\perp \cos q),$$

with positive eigenfrequencies,

$$\omega = h \left(1 - \frac{\Delta - J_\perp \cos q}{J_\perp + \Delta} \right). \tag{8}$$

Using Eqs. (4), (5), and (7), and by substituting the values of $S_l^{x,y,z}$ for a spin wave of wave vector q, we obtain, for the

spin and thermal current per unit length,

$$j_q^s = J_\perp u^2 \sin q,$$

$$j_q^\epsilon = = -2J_\perp u^2 (J_\perp \cos q - \Delta) z \sin q,$$

$$u^2 = 1 - z^2,$$

$$j_q^Q = j_q^\epsilon - h j_q^s,$$

$$j_q^Q = -\left(\frac{J_\perp(1 + \cos q)}{\Delta + J_\perp}\right) h j_q^s.$$

Thus we see that in the high-field region, for $h > 0$ the spin and thermal current have opposite sign, $j_q^Q > 0$, $j_q^s < 0$ and, of course, for $h < 0$, $j_q^Q > 0$, $j_q^s > 0$.

In the low-field antiferromagnetic region, the equations of motion are

$$\dot{S}_{2l}^x = -S_{2l}^y (2\Delta S_{\text{odd}}^z - h) + S_{\text{even}}^z J_\perp (S_{2l+1}^y + S_{2l-1}^y),$$

$$\dot{S}_{2l}^y = +S_{2l}^x (2\Delta S_{\text{odd}}^z - h) - S_{\text{even}}^z J_\perp (S_{2l+1}^x + S_{2l-1}^x),$$

$$\dot{S}_{2l+1}^x = -S_{2l+1}^y (2\Delta S_{\text{even}}^z - h) + S_{\text{odd}}^z J_\perp (S_{2l}^y + S_{2l+2}^y),$$

$$\dot{S}_{2l+1}^y = +S_{2l+1}^x (2\Delta S_{\text{even}}^z - h) - S_{\text{odd}}^z J_\perp (S_{2l}^x + S_{2l+2}^x),$$

with $S_{\text{odd,even}}^z$ the alternating S^z component at the odd and even sites. With the substitution

$$S_{2l}^x \pm i S_{2l}^y = u_\pm e^{iq2l - \omega_\pm t},$$

$$S_{2l+1}^x \pm i S_{2l+1}^y = v_\pm e^{iq(2l+1) - \omega_\pm t},$$

and taking, e.g., $S_{\text{even}}^z = +1$, $S_{\text{odd}}^z = -1$, we obtain the eigenvalue problem

$$\begin{pmatrix} \pm(2\Delta + h) & \pm 2J_\perp \cos q \\ \mp 2J_\perp \cos q & \mp(2\Delta - h) \end{pmatrix} \begin{pmatrix} u_\pm \\ v_\pm \end{pmatrix} = \omega_\pm \begin{pmatrix} u_\pm \\ v_\pm \end{pmatrix},$$

for the frequency spectrum,

$$\omega_{+\pm} = +h \pm 2\sqrt{\Delta^2 - J_\perp^2 \cos^2 q},$$

$$\omega_{-\pm} = -h \pm 2\sqrt{\Delta^2 - J_\perp^2 \cos^2 q}. \tag{9}$$

The positive frequency dispersions are $\omega_{\pm+} = \pm h + h_c \sqrt{\frac{\Delta^2 - J_\perp^2 \cos^2 q}{\Delta^2 - J_\perp^2}}$. The lower frequency dispersion ω_{-+} vanishes as $q \to 0$ at the critical field h_c, signaling the spin-flop transition.

Setting $u_- - = \cos\phi$, $v_- = \sin\phi$, $\tan\phi = \frac{-\Delta - \sqrt{\Delta^2 - J_\perp^2 \cos^2 q}}{J_\perp \cos q}$, we obtain the currents for the lower frequency dispersion,

$$j_q^s = -J_\perp u_- v_- \sin q = J_\perp \frac{J_\perp \cos q}{2\Delta} \sin q,$$

$$j_q^\epsilon = \frac{1}{2} J_\perp^2 (v_-^2 - u_-^2) \sin 2q$$

$$= \frac{1}{2} J_\perp^2 \frac{\sqrt{\Delta^2 - J_\perp^2 \cos^2 q}}{\Delta} \sin 2q,$$

$$j_q^Q = j^s \left(h_c \sqrt{1 + \frac{J_\perp^2 (1 - \cos^2 q)}{\Delta^2 - J_\perp^2}} - h\right),$$
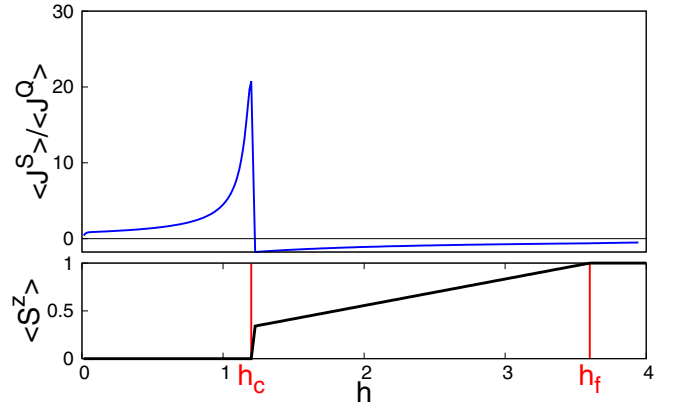
$$j_q^s / j_q^Q > 0. \tag{10}$$

FIG. 5. Spin current to thermal current ratio and magnetization as a function of magnetic field for $J_\perp = 0.8$. Average temperature $T = (T_L + T_R)/2 = 0.02$.

For the higher frequency dispersion ω_{++}, setting $u_+ = \cos\phi$, $v_+ = \sin\phi$, $\tan\phi = \frac{-\Delta + \sqrt{\Delta^2 - J_\perp^2 \cos^2 q}}{J_\perp \cos q}$, we obtain the currents

$$j_q^s = J_\perp u_+ v_+ \sin q = -J_\perp \frac{J_\perp \cos q}{2\Delta} \sin q,$$

$$j_q^\epsilon = \frac{1}{2} J_\perp^2 (u_+^2 - v_+^2) \sin 2q$$

$$= \frac{1}{2} J_\perp^2 \frac{\sqrt{\Delta^2 - J_\perp^2 \cos^2 q}}{\Delta} \sin 2q,$$

$$j_q^Q = j^s (-2\sqrt{\Delta^2 - J_\perp^2 \cos^2 q} - h),$$

$$j_q^s / j_q^Q < 0.$$

Thus, in the antiferromagnetic region, as observed in the simulations above, for $|h| < h_c$ the spin and thermal current of the dominating lower frequency dispersion spin waves have the same sign, $j_q^s / j_q^Q > 0$. We can also get a hint of the diverging behavior of $\langle J^s \rangle / \langle J^Q \rangle$ for $h \to h_c$ from Eq. (10) as at low energies for $q \to 0$, this ratio diverges.

V. "LANDAUER" APPROACH

The classical Heisenberg chain is a strongly interacting model with nonlinear equations of motion describing the spin dynamics. Therefore, we expect normal transport coefficients [16], e.g., finite thermal and spin conductivity, due to spin-wave–spin-wave scattering, although the anomalous behavior of spin transport in the isotropic Heisenberg model is presently the focus of many theoretical studies [17].

Nevertheless, for this open system with baths, we can obtain a heuristic description, shown in Fig. 5, of the spin to thermal current ratio over the whole phase diagram by considering a phenomenological "Landauer"-type model. This can be justified by the low temperature in the simulations, which implies a low spin-wave density.

Assuming that spin and energy currents are emitted at the left-right leads at temperatures $T_{L,R}$, $(\beta_{L,R} = 1/T_{L,R})$, we
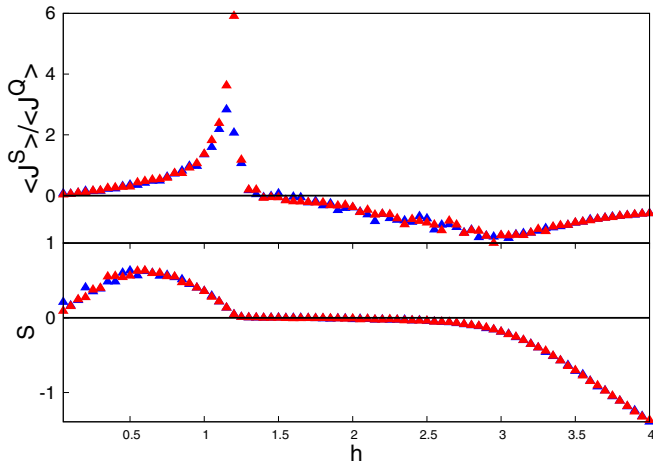
FIG. 6. Linear response coefficients as a function of magnetic field at $J_\perp = 0.8$ for $L = 160$ (blue) and $L = 320$ (red) at temperature $T = 0.05$.

obtain, for $h < h_c$ (antiferromagnetic region),

$$\langle J^S \rangle = \sum_\pm \int_0^{+\pi/2} \frac{dq}{2\pi} \left(n_{\pm q}^L - n_{\pm q}^R \right) j_{\pm q}^s,$$

$$\langle J^Q \rangle = \sum_\pm \int_0^{+\pi/2} \frac{dq}{2\pi} \left(n_{\pm q}^L - n_{\pm q}^R \right) j_{\pm q}^Q,$$

summing the contributions over the positive frequency dispersions (9) with $n_{\pm q}^{L,R} = 1/(e^{\beta_{L,R}\omega_{\pm q}} - 1)$ (here we assume for simplicity a bosonic thermal distribution function). Similar expressions are obtained for $h > h_c$ summing over the positive frequency dispersion (8).

VI. LINEAR RESPONSE

Last but not least, in linear response, the spin and thermal currents are related by transport coefficients C_{ij},

$$\begin{pmatrix} J^Q \\ J^S \end{pmatrix} = \begin{pmatrix} C_{QQ} & C_{QS} \\ C_{SQ} & C_{SS} \end{pmatrix} \begin{pmatrix} -\nabla T \\ \nabla h \end{pmatrix}, \qquad (11)$$

where $C_{QQ} = \kappa_{QQ}$ ($C_{ss} = \sigma_{ss}$) is the heat (spin) conductivity. The coefficients C_{ij} are given by the thermal average of time-dependent current-current correlation functions in a closed system with periodic boundary conditions,

$$C_{i,j} = \frac{1}{L} \int_0^\infty dt \langle J^i(t) J^j(t = 0) \rangle.$$

The time dependence is obtained by the same molecular dynamics procedure (3) after equilibrating the system at a given temperature and then switching off the thermal noise. In Fig. 6, we show two situations: (i) a system with no spin accumulation by setting $\nabla h = 0$, relevant to an open system and (ii) a system with no spin current, $\langle J^S \rangle = 0$, giving the spin Seebeck coefficient $S = \frac{\nabla h}{\nabla T} = \frac{C_{SQ}}{C_{SS}}$. For the open system, we find the same behavior of $\langle J^S \rangle / \langle J^Q \rangle$ as in the MD simulations.

VII. CONCLUSIONS

We have studied the spin Seebeck effect in the simplest prototype classical easy-axis magnetic chain model by molecular dynamics simulations and basic spin-wave theory. We have found a sign change at the spin-flop transition and clarified the role of spin-wave excitations in the low-field antiferromagnetic phase as well as in the high-field ferromagnetic phase. This classical model could be realized experimentally in quasi-one-dimensional large spin compounds, but also provides a guide to the spin Seebeck effect studied over many years in bulk magnetic materials. The observations of this study should be extended to quantum spin systems, as the spin-1/2 easy-axis Heisenberg model, where the integrability of the model [15] allows an exact evaluation of the spin Seebeck coefficient. The scope is to assess the potential of the large variety of spin chain materials for spintronic applications.

[1] S. Maekawa, T. Kikkawa, H. Chudo, J. Ieda, and E. Saitoh, J. Appl. Phys. **133**, 020902 (2023).

[2] T. Kikkawa and E. Saitoh, Annu. Rev. Condens. Matter Phys. **14**, 129 (2023).

[3] S. M. Wu, W. Zhang, A. KC, P. Borisov, J. E. Pearson, J. S. Jiang, D. Lederman, A. Hoffmann, and A. Bhattacharya, Phys. Rev. Lett. **116**, 097204 (2016).

[4] J. Li, C. B. Wilson, R. Cheng, M. Lohmann, M. Kavand, W. Yuan, M. Aldosary, N. Agladze, P. Wei, M. S. Sherwin, and J. Shi, Nature (London) **578**, 70 (2020).

[5] J. Li, H. T. Simensen, D. Reitz, Q. Sun, W. Yuan, C. Li, Y. Tserkovnyak, A. Brataas, and J. Shi, Phys. Rev. Lett. **125**, 217201 (2020).

[6] W. Yuan, J. Li, and J. Shi, Appl. Phys. Lett. **117**, 100501 (2020).

[7] S. M. Rezende, R. L. Rodríguez-Suárez, and A. Azevedo, Phys. Rev. B **93**, 014425 (2016).

[8] Y. Yamamoto, M. Ichioka, and H. Adachi, Phys. Rev. B **100**, 064419 (2019).

[9] D. Reitz, J. Li, W. Yuan, J. Shi, and Y. Tserkovnyak, Phys. Rev. B **102**, 020408(R) (2020).

[10] Y. Yamamoto, M. Ichioka, and H. Adachi, Phys. Rev. B **105**, 104417 (2022).

[11] D. Reitz and Y. Tserkovnyak, arXiv:2307.02734.

[12] H. J. Mikeska and M. Steiner, Adv. Phys. **40**, 191 (1991).

[13] D. Hirobe, M. Sato, T. Kawamata, Y. Shiomi, K. Uchida, R. Iguchi, Y. Koike, S. Maekawa, and E. Saitoh, Nat. Phys. **13**, 30 (2017).

[14] Y. Chen, M. Sato, Y. Tang, Y. Shiomi, K. Oyanagi, T. Masuda, Y. Nambu, M. Fujita, and E. Saitoh, Nat. Commun. **12**, 5199 (2021).

[15] C. Psaroudaki and X. Zotos, J. Stat. Mech. (2016) 063103.

[16] A. V. Savin, G. P. Tsironis, and X. Zotos, Phys. Rev. B **72**, 140402(R) (2005).

[17] Google Quantum AI and Collaborators, arXiv:2306.09333.

[18] J. L. García-Palacios and F. J. Lazaro, Phys. Rev. B **58**, 14937 (1998).

[19] F. Naef and X. Zotos, J. Phys. Condens. Matter. **10**, L183 (1998).

[20] F. Heidrich-Meisner, A. Honecker, and W. Brenig, Phys. Rev. B **71**, 184415 (2005).